The International Journal of Advanced Manufacturing Technology (2018) 99:613–622
https://doi.org/10.1007/s00170-018-2424-9

ORIGINAL ARTICLE

Numerical and experimental investigations on temperature distribution of plain-woven aramid fiber-reinforced plastics composites with low-mild spindle velocities

Yong-Jie Bao[1,2] · Wei Hao[2] · Hang Gao[2] · Xue-Shu Liu[2] · Yi-Qi Wang[2]

Received: 22 September 2017 / Accepted: 16 July 2018 / Published online: 7 August 2018

Abstract
Temperature distribution of plain-woven aramid fiber-reinforced plastics (AFRP) composites was investigated by numerical and experimental methods for their drilling process with low-mild spindle velocities. A three-dimensional (3-D) numerical model was proposed for predicting the temperature distribution. Drilling experiments were carried out to verify the proposed numerical model and investigate the thermal damages with low-mild spindle velocities. The accuracy of the proposed numerical model was acceptable with less than 8% relative errors compared with experimental results. Cutting heat easily accumulated even the AFRP composites were drilled with low-mild spindle velocities for their poor thermal conductivity. Temperature distributions presented a rounded diamond shape, which diagonal direction was consistent with the fiber direction. With the high heat accumulation, although the drilled hole wall was damaged by the high temperature, carbonation phenomenon was not serious for the low spindle velocity drilling. For the mild spindle velocity drilling case, a serious carbonation phenomenon had been observed, and the heat-affected layer in the hole wall was about 0.3 mm.

Keywords Plain-woven AFRP composites · Temperature distribution · Drilling · Low-mild spindle velocity

1 Introduction

Due to their high strength, low density, and good impact resistance, aramid fiber/epoxy composite materials have been widely used in aviation industry. Generally, single composite component can be manufactured with a near-net shape. There are very few or even no more processing demands for the single component. Although adhesive joining method is used in aviation industry, mechanical joining is very common to assemble the composite components together by using blots and rivets. To realize the further mechanical joining, drilling is one of the most common operations [1]. The superior properties of composite materials make difficulties for the drilling process. It always induces burrs, delamination, and thermal damage, and so on, which are detrimental to the quality of the composite materials. Those defects cause many negative effects in reducing the strength and fatigue life of composite materials [2]. Due to the high local flexibility and toughness of aramid fibrils, the machined quality of aramid fiber-reinforced plastics (AFRP) composites is worse than that of carbon fiber-reinforced plastics (CFRP) composites [3].

Aramid fiber is a kind of strong and heat-resistant fiber having high toughness and low thermal conductivity. Moreover, by considering the maintenance of the chemical-physical characteristics of resins, refrigerant fluid is usually not allowed to be used during the machining of composite components [4]. Thus, for a dry drilling process of AFRP composites, it is difficult to disperse the heat generated by cutting edges due to aramid fiber's low thermal conductivity. The large amount of heat may accumulate to raise the temperature of the composite materials, which can soften resin and then the resin adheres to the tool. When the temperature exceeds the critical degradation temperature of the epoxy-based matrix, thermal degradation processes can be triggered [5]. And as the temperature rises gradually and exceeding the glass transition temperature (T_g) of epoxy resin (about 200 °C),

✉ Yi-Qi Wang
wangyiqi@dlut.edu.cn

[1] Engineering Training Center, Dalian University of Technology, Dalian 116024, The People's Republic of China

[2] Key Laboratory for Precision and Non-Traditional Machining Technology of Ministry of Education, School of Mechanical Engineering, Dalian University of Technology, Dalian 116024, The People's Republic of China

strength, elastic modulus, and other mechanical properties of the resin and composites decrease sharply [6]. All these negative influences are caused by the very low thermal conductivity of aramid fiber in the composites.

Many researchers have studied drilling AFRP composites, which are focusing on the drilling mechanisms, processing technologies, machining tools, cutting parameter optimization, etc. Bhattacharyya and Horrigan [7] extended the investigation of drilling Kevlar fiber-reinforced plastic (KFRP) composites and the effects of different cutting variables on the quality of drilled holes at both ambient and cryogenic temperatures. Gao et al. [8] proposed a combined machining technology based on sawing and grinding mechanisms and achieved damage-free machining quality for AFRP composites. Shuaib et al. [9] studied the machinability of Kevlar 49 laminates using TiN-coated high-speed steel (HSS) drills under different composite preparation parameters and drilling conditions. Zheng et al. [10] carried out an experimental study of drilling the ceramics/KFRP double-plate composite armor by using a special sintering diamond core drill. El-Taweel et al. [11] focused on the cutting performance of a CO_2 laser on KFRP composites and used the Taguchi method to optimize laser control parameters.

Besides, many researches have been carried out by using experimental and numerical methods to investigate the machining temperature effects of AFRP composites. Wang et al. [12] analyzed the influence of low-temperature conditions. They found that temperature drop has played a positive role to reduce the cutting defects of AFRP composites. Sorrentino et al. [13] developed a sensory system for the in-process monitoring of the temperature near the machined surface and on the tool during dry drilling of FRP laminates. Yilbas and Akhtar [14] used the finite element code ABAQUS to propose a laser drilling model for Kevlar laminates composites. They predicted the temperature and stress fields along the cutting sections. Bao et al. [15] developed a drilling temperature model based on the finite difference method (FDM). In addition, they analyzed the characteristics of temperature field during drilling unidirectional Kevlar composites. Sadek et al. [16] developed a novel hybrid analytical-numerical model to capture time-varying forces and temperatures during transient and steady-state drilling of FRPs. Generally, the prediction of the temperature distribution in the workpiece can provide useful information for optimizing the cutting process.

To obtain better quality, high velocity is usually used for drilling fiber-reinforced composites. The drilling quality of CFRP composite can be improved by increasing the spindle velocity according to the research by Tsao and Hocheng [17]. However, the low and anisotropy thermal conductivity of AFRP composites makes the cutting heat rise and the cutting damages occur easily with high spindle velocity. It is necessary to reveal the characteristic of the cutting heat rising and the temperature distribution during drilling process, which can assist other researchers for further understanding their machining process and mechanisms.

A 3-D numerical model was proposed to investigate the temperature distribution of plain-woven AFRP composites while they were drilled with low-mild spindle velocities. Experiments were carried out to verify the proposed numerical model by monitoring the single-point and lower surface temperature distribution at the exit of drilled hole. The effects of cutting heat on drilling quality were studied as well.

2 3-D numerical model

2.1 Homogenization hypothesis of thermophysical parameters

The plain-woven AFRP composites contain 25 layers, and thickness (t) of each layer is 0.2 mm. Thus, the total thickness of composites is 5 mm. To simplify the model for numerical calculation, it hypothesized that:

(1) There is no defect in AFRP composites.
(2) The plain-woven aramid fabric is treated as two unidirectional plates, whose fiber directions are perpendicular to each other, and thickness of each unidirectional plate is $t/2$ as shown in Fig. 1.
(3) Aramid fibers are uniformly aligned in the composites.

Compared with steel, the thermal conductivity of plain-woven AFRP composites is dramatically low, even lower than

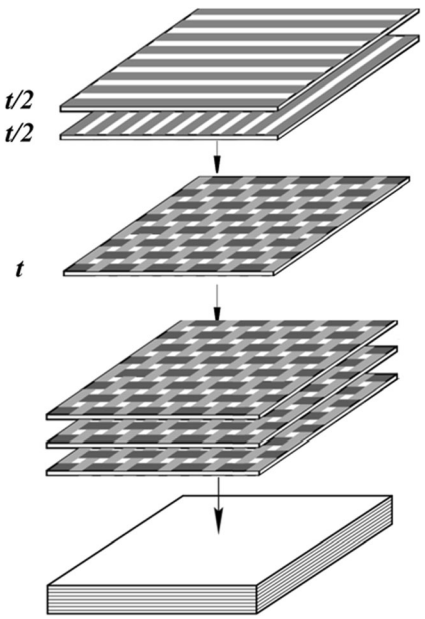

Fig. 1 A simplified model for the plain-woven AFRP composite

that of CFRP composites. The thermal conductivity along the aramid fibers is higher than that perpendicular to the fiber direction. The thermophysical parameters of composites are supposed to be homogenized according to the volume of fiber and resin [18]. Based on the rule of mixture, the density and specific heat capacity of aramid fiber and resin were calculated by Eq. 1 and Eq. 2. Based on the effective-medium theory, thermophysical parameters along the fiber direction and perpendicular to the fiber direction can be calculated as Eq. 3 and Eq. 4 [19].

$$\rho = \rho_f \times V_f + \rho_r \times \left(1-V_f\right) \tag{1}$$

$$c = c_f \times V_f + c_r \times \left(1-V_f\right) \tag{2}$$

$$k_l = k_f \times V_f + k_r \times \left(1-V_f\right) \tag{3}$$

$$k_t = \left(\frac{V_f}{k_f} + \frac{1-V_f}{k_r}\right)^{-1} \tag{4}$$

where ρ and c are the density and volume specific heat of plain-woven AFRP composites, k represents the thermal conductivity, and V represents the volume fraction. The subscripts f and r, respectively, refer to aramid fiber and resin. The subscripts l and t represent the longitude and transverse thermal conductivity of plain-woven AFRP composites. After homogenizing, the thermophysical properties of plain-woven AFRP composites are shown in Table 1.

2.2 Establish the 3-D numerical model

A 3-D numerical model was proposed based on the FDM to investigate the temperature distribution of drilling process for plain-woven AFRP composites. For simplification, as shown in Fig. 2, the upper and lower surfaces are regarded as convective boundaries while the rest four surfaces are taken as adiabatic surfaces. Heat flux load q_1 is induced by the major cutting edges, which can be considered as a moving conical heat source. Meanwhile, the side edges can generate q_2. Because the side edges only play a guiding role in drilling, and the value of q_2 is very small, q_2 is ignored in the 3-D numerical model. Compared with solid heat conduction, thermal radiation is also ignored for its low value.

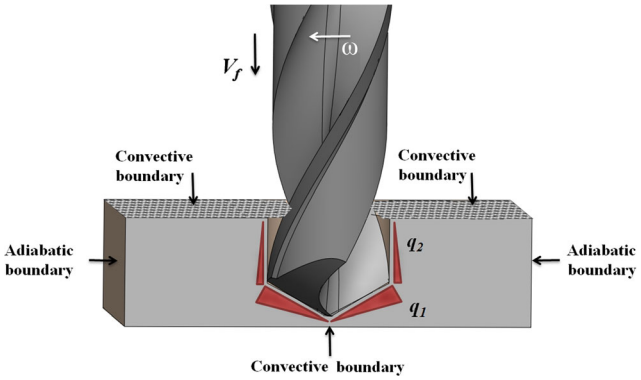

Fig. 2 Schematic of the numerical model for drilling AFRP composites

The step size along three directions of x, y, and z is set as $\triangle x$, $\triangle y$, and $\triangle z$, respectively. The time step is set as $\triangle t$.

$$\begin{cases} x = i\cdot\Delta x, \ i\in[0, N_x] \\ y = j\cdot\Delta y, \ j\in[0, N_y] \\ z = k\cdot\Delta z, \ k\in[0, N_z] \\ t = n\cdot\Delta t, \ n\in[0, N_t] \end{cases} \tag{5}$$

where Nx, Ny, and Nz are the mesh numbers in the three directions, respectively, Nt is the mesh number of the time.

Most of the consuming energy is converted to heat conducting to the workpiece, chip, tool, and the surrounding environment. The average heat flux q_0 is shown as follows [20]:

$$q_0 = \frac{\eta\left(M\cdot\omega + F_z\cdot v_f\right)}{\pi\left(\frac{d}{2}\right)^2/\sin 59^\circ} \tag{6}$$

where η is the energy proportional coefficient, M and F_z are the torque and the thrust force, ω and v_f are the angular velocity and feed velocity of the drill, and d is the diameter of the drill. The above parameters can be determined according to experimental settings.

Table 1 The thermophysical properties of plain-woven AFRP composites

Thermophysical parameters	Symbol	Value
Thermal conductivity of aramid fiber 49 (W m^{-1} K^{-1})	k_f	1.365
Thermal conductivity of epoxy resin (W m^{-1} K^{-1})	k_r	0.15
Fiber volume fraction (%)	V_f	60
Density of the plain-woven AFRP composite (kg m^{-3})	ρ	1444
Specific heat capacity (J kg^{-1} K^{-1})	c	1398.46
Longitude thermal conductivity (W m^{-1} K^{-1})	k_l	0.879
Transverse thermal conductivity (W m^{-1} K^{-1})	k_t	0.322

The upper and lower surfaces are convective boundaries. The boundary conditions and difference forms are written as follows:

$$h \cdot T = k_z \frac{\partial T}{\partial z} \quad (z = 0, l_z) \tag{7}$$

$$\begin{cases} h \cdot T^n_{i,j,1} = k_z \dfrac{T^n_{i,j,1} - T^n_{i,j,2}}{\Delta z} \\ h \cdot T^n_{i,j,N_z} = k_z \dfrac{T^n_{i,j,N_z} - T^n_{i,j,N_z-1}}{\Delta z} \end{cases} \tag{8}$$

where h is the heat transfer coefficient.

The rest four surfaces are taken to be insulating. The difference forms are written as follows:

$$\begin{cases} T^n_{i+1,j,k} = T^n_{i,j,k}, i = 0 \cup (N_x - 1) \\ T^n_{i,j+1,k} = T^n_{i,j,k}, j = 0 \cup (N_y - 1) \end{cases} \tag{9}$$

The initial condition of each node of the numerical model is written as follows:

$$T^0_{i,j,k} = T_0 \quad i \in [0, N_x], j \in [0, N_y], k \in [0, N_z] \tag{10}$$

During the drilling process, the temperature distribution is a non-steady-state along with the heat accumulating. The heat conduction equation of three-dimensional mode can be written as follows:

$$k_x \frac{\partial^2 T}{\partial x^2} + k_y \frac{\partial^2 T}{\partial y^2} + k_z \frac{\partial^2 T}{\partial z^2} + q(x, y, z) = \rho c \frac{\partial T}{\partial t} \tag{11}$$

where k_x, k_y, and k_z are the thermal conductivities in the three directions, respectively. $q(x, y, z)$ is a heat flux, and T is the relative temperature rise. The thermal conductivity alternates by the fiber direction from 0° to 90° continuously while the drill goes down. In order to adapt the FDM to programming, the heat conduction equation and boundary conditions are written in difference forms [15].

3 Experimental details

3.1 Materials and experimental setup

The plain-woven AFRP composite contained 60 vol.% Kevlar-49 fiber and 40 vol.% diglycidyl 4,5-epoxy tetrahydro phthalate (TDE-85), which are used as the reinforcement and matrix, respectively. The glass transition temperature of TDE-85 is about 185 °C. The drilling tool was made of cemented carbide with a diameter of 6.5 mm and a point angle of 118°. Besides, the projection length of the main cutting edge in the drill core line is 1.5 mm.

The schematic of the experimental setup is shown in Fig. 3 for drilling AFRP composites. The cutting force was measured by Kistler 9271A dynamometer, and all data were collected. The Thermo-Vision™ A40-M infrared thermometer (FLIR® Systems Inc., USA) was used to measure temperature distribution at the exit of the hole. Three K-type thermocouples were embedded at a depth of 0.6 mm from the exit in order to monitor the temperature rise during drilling process. AFRP composites were drilled with a constant feed rate of 2 mm min^{-1} under low-mild spindle velocities, which were 1000 r min^{-1} and 3000 r min^{-1}, respectively. Moreover, the surface morphologies and microstructures of the drilled

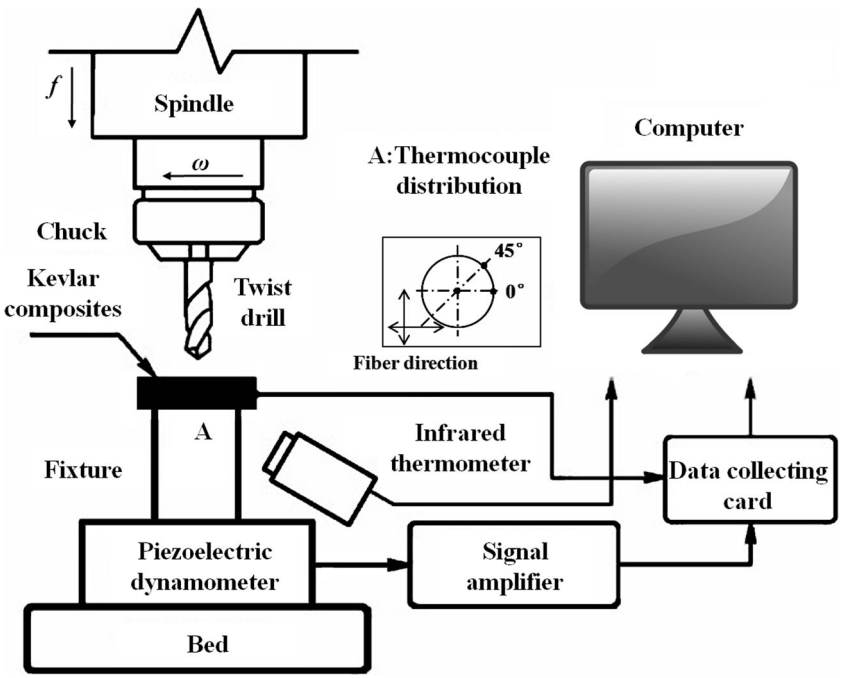

Fig. 3 Schematic of the experimental setup for drilling AFRP composites

specimens were observed by using the digital microscope VHX-600E and the scanning electron microscope (SEM) FEI Q45.

3.2 Input parameters for numerical simulation

The drilling experiments of plain-woven AFRP composites were carried out under the condition of dry machining. Relevant input parameters for simulation such as torque and thrust were determined based on the experiments. The drilling process was performed in a natural convection environment. The heat transfer coefficient h was set as 20 W m^{-2} K^{-1} [21]. The initial room temperature was at 16 °C. Moreover, the proportional coefficient of energy (η) for improving the accuracy of the proposed model was set as 18% by fitting experimental data. Load parameters obtained from experiments for numerical simulation are shown in Table 2.

4 Results and discussion

4.1 Single-point temperature rise

Drilling is a semi-closed machining process. Cutting heat is accumulating while the drill goes down. In order to explore the characteristic of temperature rise with low and anisotropic thermal conductivity in the material, three points inside the material were selected to monitor the temperature rise by K-type thermocouple. As shown in Fig. 4, the three points were set at the hole center, 0° direction of hole wall, and 45° direction of hole wall, respectively. The K-type thermocouples were placed in the AFRP composite materials with a distance 0.6 mm from the lower surface.

Under the spindle velocity of 1000 r min^{-1} and feed speed of 2 mm min^{-1}, the measured time-temperature curves at different locations are shown in Fig. 4. Generally, temperature was increasing continuously with the drill closing the monitored points. This was caused by the heat accumulation and thermal transmission in the AFRP composites during the drilling process. At the early stage of drilling, the temperature rise

Table 2 Input parameters obtained from experiments for numerical simulation

Parameters	Symbols	Values
Spindle velocity (r min^{-1})	n	1000/3000
Feed rate (mm min^{-1})	v_f	2
Torque (N m)	T	0.045/0.025
Thrust force (N)	Fz	40/20
Heat transfer coefficient (W m^{-2} K^{-1})	h	20
Proportional coefficient of energy (%)	η	18

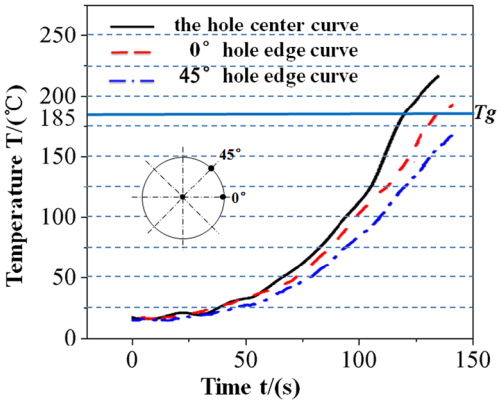

Fig. 4 Measured time-temperature curves at different locations with a low spindle velocity of 1000 r min^{-1}

was not obvious because little heat was accumulated and there was a distance between the thermocouples and the drilling tool. Because the heat generated is faster than that loss, thus, as closing to the measuring point, slopes of curves increased a lot. Moreover, the maximum value of temperature was obtained when the drill reached the positions of thermocouples. As shown in Fig. 4, the temperature in the hole center is larger than that of the others because more than 50% of the cutting force comes from the chisel edge of the drill. Due to the fiber orientation effects, the temperature along the 0° direction of hole wall rose more quickly than that along the 45° direction of hole wall. It was found that the temperature was higher than T_g of resin matrix after about 120 s, which meant that cured matrix would be softened.

The numerical model was established by the FDM to simulate the temperature rise curves at drill exit. As shown in Fig. 5, the curves predicted by simulations had a good agreement with the experimental results. At the center of the hole, the measured and predicted highest temperatures were 220 °C and 211.7 °C, respectively, which meant a simulation error of 3.77%. Besides, the measured and predicted highest temperatures parallel to the fiber were 190 °C and 175.3 °C, respectively, which meant a simulation error of 7.74%. In some recent research works, the estimation errors are in the range of 7–18% [22–24]. The simulation errors are less than 8% by using our proposed model; thus, the accuracy of this numerical model is acceptable.

4.2 Simulation of temperature distribution

During the drilling of plain-woven AFRP composites, four particular stages of the drilling process were presented for discussing the processes of heat generation and thermal transmission. Four stages are defined according to the feed of chisel edge at 0.5 mm (stage 1), 1.5 mm (stage 2), 5.0 mm (stage 3), and 6.5 mm (stage 4) away from the top surface of composites in thickness direction. At the spindle velocity of 1000 r min^{-1}, the temperature distributions of these four

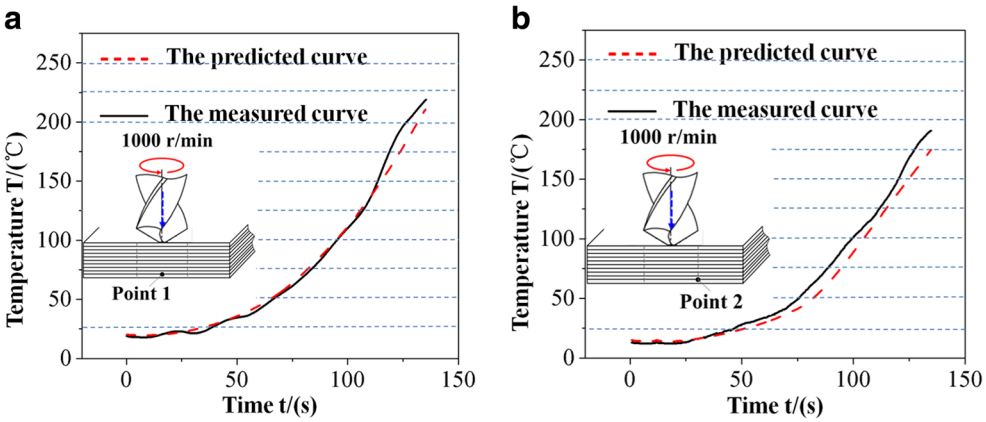

Fig. 5 Time-temperature curves with a low spindle velocity of 1000 r min^{-1}. **a** Point 1 (hole center). **b** Point 2 (0° hole edge)

typical moments are shown in Fig. 6. The temperature distribution during the machining process was different from that of the homogeneous material obviously [25]. It also differed from the CFRP composites, which has an elliptical shape according to the research by Zhu et al. [26]. The temperature along the 0° and 90° direction rose more quickly than the 45° direction, which was consistent with the characteristics of the single-point. The temperature distribution showed a rounded diamond shape whose diagonal directions were consistent with the fiber directions. The reason can be explained as follows: the thermal conductivity along the aramid fiber axis is the maximum and the thermal conductivity of the resin matrix is only 0.15 W m^{-1} K^{-1}, which is much lower than that of the aramid fiber. Thus, the cutting heat is mainly transferred

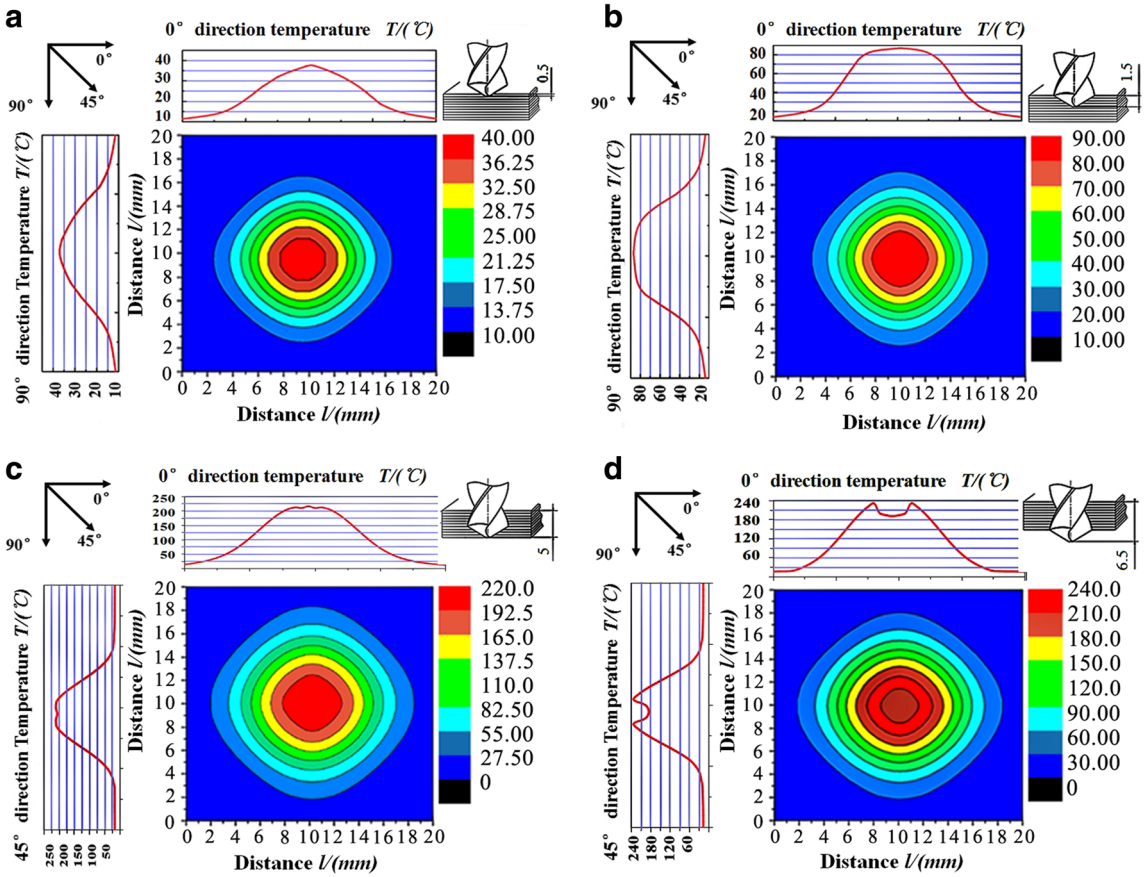

Fig. 6 Temperature distributions of four stages with a low spindle velocity of 1000 r min^{-1}. **a** 0.5 mm (stage 1). **b** 1.5 mm (stage 2). **c** 5 mm (stage 3). **d** 6.5 mm (stage 4)

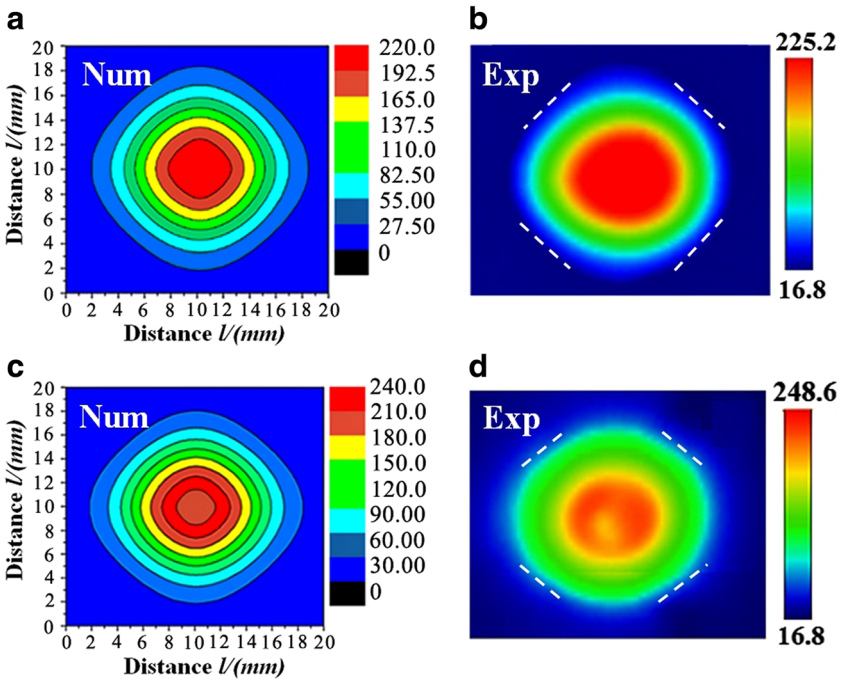

Fig. 7 Temperature distributions with a low spindle velocity of n = 1000 r min^{-1}. **a** Numerical result for 5 mm away from the top. **b** Experimental result for 5 mm away from the top. **c** Numerical result for 6.5 mm away from the top. **d** Experimental result for 6.5 mm away from the top

through the aramid fiber. In other words, the anisotropic thermal conductivity plays a key role to the temperature distribution.

As shown in Fig. 6a, the higher temperature area for drilling 0.5-mm depth was at the center of the hole, and the predicted highest temperature was 39.8 °C. The material was mainly removed by chisel edge for this stage. The short contact time and small contact area were the reason that thrust force and torque were not high enough to cause a significant increase in temperature. When the drill moved down and reached 1.5 mm away from the top surface, the main cutting edges began to participate fully in the cutting. Thus, the highest temperature rose up to 88.2 °C and the area affected by the heat was enlarged, which is shown in Fig. 6b. Compared with the first stage, the temperature at the center of the hole increases significantly. The temperature distribution of exit when the chisel edge just reached the bottom is shown in Fig. 6c. The maximum temperature was 216.4 °C, which was higher than the T_g of resin. With such a high temperature, the resin matrix was softened. It could result in a rapid decline in the mechanical properties of AFRP composites. After this stage, cutting edges started to move outside. Figure 6d shows the temperature distribution of exit when the main cutting edges were just out of processing totally. The maximum predicted temperature was 232 °C, which was a little higher than the third stage. The higher temperature area was no longer at the center of the hole, but appeared at the side area of main cutting edges because the chisel edge was no longer involved in cutting and it had a good thermal conductivity.

4.3 Verification of temperature distribution

Drilling experiments were carried out for further verification of the proposed numerical model. Because stage 3 and stage 4 were easily monitored by using an infrared thermometer, thus, these two typical moments were selected to be discussed. The

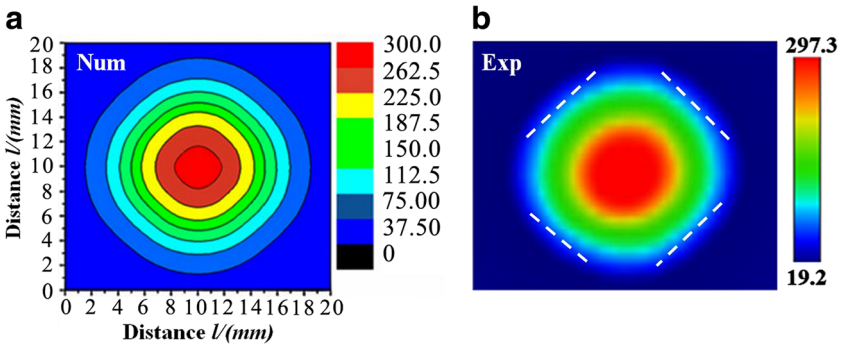

Fig. 8 Temperature distributions for 5 mm away from the top with a mild spindle velocity of n = 3000 r min^{-1}. **a** Numerical result. **b** Experimental result

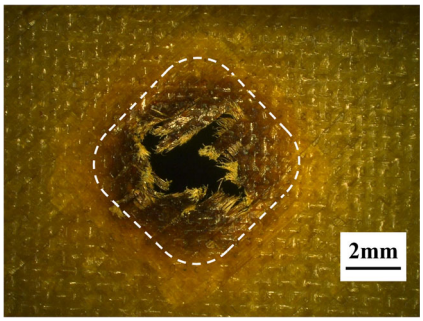

Fig. 9 Rounded diamond feature of the exit drilled at a low spindle velocity 1000 r min^{-1}

comparison results between simulation and experiments with a low spindle velocity of 1000 r min^{-1} are shown in Fig. 7.

The temperature distributions of simulation and experiment are shown in Fig. 7a, b for stage 3, when the chisel edge just reached to the bottom of AFRP composites. The higher temperature area was at the center of the hole, and the measured highest temperature of simulation was 216.4 °C as shown in Fig. 7a. The maximum temperature of the experiment was 225.2 °C as shown in Fig. 7b. The relative temperature error was close to 3.9%. For stage 4, the maximum temperatures of simulation and experiment were 232 °C and 248.6 °C, respectively, which relative temperature error was close to 6.7%. Moreover, the temperature distributions of simulations and experiments are well matched to each other for both stage 3 and stage 4. The temperature distributions predicted by using the proposed numerical model have a good agreement with that of experimental results.

Similar experiments were performed with a mild spindle velocity of $n = 3000$ r min^{-1}. The temperature distributions of simulation and experiment for stage 3 are shown in Fig. 8. A similar temperature distribution trend was confirmed by comparing it with the case at a low spindle velocity of 1000 r min^{-1}. The highest predicted and measured temperatures were 285.6 °C and 297.3 °C, respectively. The relative temperature error between simulation and experiment was close to 3.9%. Comparing Fig. 7b with Fig. 8b, experimental results showed that the highest temperature increased more than 70 °C when the spindle velocity increases from 1000 to 3000 r min^{-1}. Moreover, while the drill reached near the

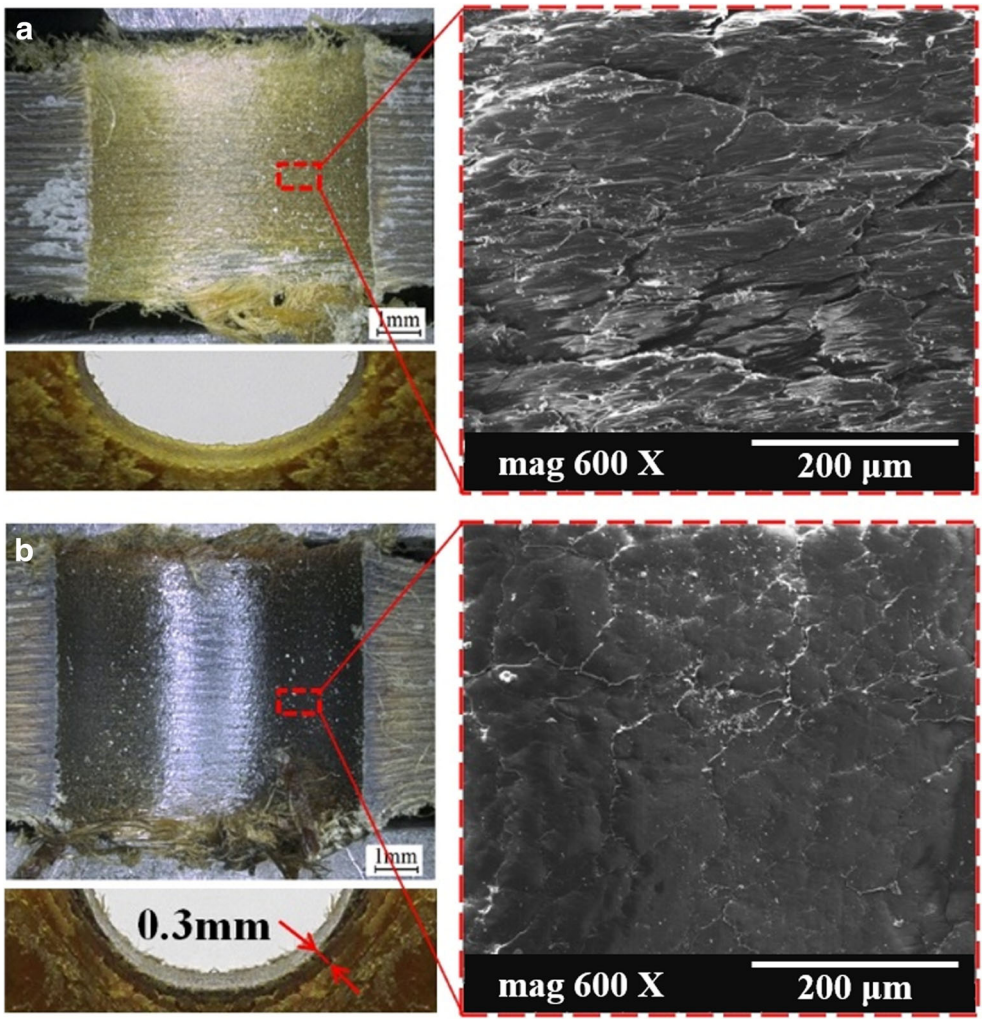

Fig. 10 **a** Surface morphologies of hole wall at low spindle velocity of $n = 1000$ r min^{-1}. **b** Surface morphologies of hole wall at middle spindle velocity of $n = 3000$ r min^{-1}

bottom of the composites, the carrying capacity decreased with the uncut layers reducing. Therefore, defects, especially delamination, were more likely to occur at this stage during drilling composites with twist drill according to the study by Hocheng and Tsao [27]. Especially, the maximum temperature was higher than the T_g of the resin matrix.

4.4 Thermal damage and drilling quality

During drilling process of plain-woven AFRP composites, even at the low spindle velocity 1000 r min^{-1} with a feeding rate of 2 mm min^{-1}, heat accumulated rapidly because of the low thermal conductivity. As shown in Figs. 4 and 7, before the chisel edge reached to the bottom of plain-woven AFRP composites, the highest temperature of the cutting area exceeded the T_g of the resin matrix. Then, the bonding strength of the resin was decreased, and the integrity of the machined surface at the drill exit worsened as shown in Fig. 9. Thermal damage and color change of drilled plain-woven AFRP composites were easily observed due to the excessive temperature. The thermal damage zone presented a rounded diamond shape, which was consistent with the predicted shapes of temperature distributions in Figs. 6, 7, and 8.

Surface morphologies of hole wall at low-mild spindle velocities of n = 1000 r min^{-1} and n = 3000 r min^{-1} are shown in Fig. 10. Due to high toughness of aramid fiber, long fiber burrs were found at the entrance and exit areas for both cases. As shown in Fig. 10a, although the spindle velocity was only at 1000 r min^{-1}, the carbonation phenomenon was identified by the color changing, which was also proved by the SEM image (right) of Fig. 10a with the melted sign of the resin matrix. It also presented many micro cracks in the machined hole wall. As shown in Fig. 10b, the serious carbonation phenomenon was found for its distinct dark color when spindle velocity increased to 3000 r min^{-1}. Moreover, the thickness of the burned layer was about 0.3 mm as shown in Fig. 10b (left bottom). The surface of hole wall was much more compacted with few micro cracks as shown in Fig. 10a (right). Higher spindle velocity accumulated more heat, which resulted in damages that were more serious.

5 Conclusions

Temperature distribution of plain-woven AFRP composites was investigated by numerical and experimental methods for their drilling process with low-mild spindle velocities. A 3-D numerical model was proposed to predict the temperature distribution of AFRP composites for their drilling process. Four typical moments of drilling process were discussed. To verify the numerical model, single-point measurement was applied for monitoring the local temperature by using K-type thermocouples and temperature distributions of lower surface at the exit of drilled hole were observed by using an infrared thermometer. Several conclusions have been summarized as follows:

(1) The transmission of cutting heat in 0° direction (along fiber axis) is faster than that in 45° direction obtained by the single-point measurement. The simulations have a good agreement with the experimental results, and the relative errors are less than 8%, which means the accuracy of numerical model is acceptable.
(2) The temperature distributions present a rounded diamond shape, which diagonal direction is consistent with the fiber direction.
(3) Although low-mild spindle velocities were applied to drill AFRP composites, heat still can easily accumulate for their poor thermal conductivity. The maximum temperature was higher than T_g of the resin matrix, combined with high toughness aramid fibers, which resulted in many fiber burrs.
(4) With the high heat accumulation, although the drilled hole wall is damaged by the high temperature, carbonation phenomenon is not serious for the low spindle velocity drilling. For the mild spindle velocity drilling case, a serious carbonation phenomenon has been observed, and the heat-affected layer in hole wall is about 0.3 mm.

Funding information This research was supported by the National Natural Science Foundation of China (NSFC) [grant numbers 51475073, 51375068, 51605076]; the National Key Basic Research Program of China (973 Project) [grant number 2014CB046504]; and the Fundamental Research Funds for the Central Universities [grant number DUT16QY01].

References

1. Karpat Y, Degerb B, Bahtiyar O (2012) Drilling thick fabric woven CFRP laminates with double point angle drills. J Mater Process Technol 212:2117–2127
2. Persson E, Eriksson I, Zackrisson L (1997) Effects of hole machining defects on strength and fatigue life of composite laminates. Compos Part A 28A:141–151
3. Won MS, Dharan CKH (2002) Drilling of aramid and carbon fiber polymer composites. J Manuf Sci Eng 124:778–783
4. Sorrentino L, Turchetta S, Colella L, Bellini C (2016) Analysis of thermal damage in FRP drilling. Process Eng 167:206–215
5. Chatterjee A (2009) Thermal degradation analysis of thermoset resins. J Appl Polym Sci 114:1417–1425
6. Zhu DJ, Zhang XT, Zhang HA (2016) Effects of strain rate and temperature on mechanical properties of Kevlar 49 aramid fabric reinforced epoxy polymers under dynamic tensile loading. Acta Materiae Compositae Sinica 33:459–468
7. Bhattacharyya D, Horrigan DPW (1998) A study of hole drilling in Kevlar composites. Compos Sci Technol 58:267–283

8. Gao H, Zhuang Y, Wang B, Huang JL (2012) Study on the combined machining technology of sawing and grinding for drilling aramid/epoxy composites. Adv Mater Res 565:436–441
9. Shuaib AN, Al-Sulaiman FA, Hamid F (2004) Machinability of Kevlar 49 composite laminates while using standard TiN coated HSS drills. Mach Sci Technol 8:449–467
10. Zheng L, Zhou H, Gao C, Yuan JT (2012) Hole drilling in ceramics/Kevlar fiber reinforced plastics double-plate composite armor using diamond core drill. Mater Des 40:461–466
11. El-Taweel TA, Abdel-Maaboud AM, Azzam BS, Mohammad AE (2009) Parametric studies on the CO_2 laser cutting of Kevlar-49 composite. Int J Adv Manuf Technol 40:907–917
12. Wang FB, Wang YQ, Hou B, Zhang JB, Li YP (2016) Effect of cryogenic conditions on the milling performance of aramid fiber. Int J Adv Manuf Technol 83:429–439
13. Sorrentino L, Turchetta S, Bellini C (2017) In process monitoring of cutting temperature during the drilling of FRP laminate. Comp Struct 168:49–561
14. Yilbas BS, Akhta SS (2012) Laser cutting of Kevlar laminates and thermal stress formed at cutting sections. Opt Laser Eng 50:204–209
15. Bao YJ, Zhang YN, Gao H, Liu XS (2015) Temperature field study of hole drilling in Kevlar composites. Adv Mater Res 1136:215–220
16. Sadek A, Shi B, Meshreki M, Duquesne J, Attia MH (2015) Prediction and control of drilling-induced damage in fibre-reinforced polymers using a new hybrid force and temperature modelling approach. CIRP Ann Manuf Technol 64:89–92
17. Tsao CC, Hocheng H (2008) Evaluation of thrust force and surface roughness in drilling composite material using Taguchi analysis and neural network. J Mater Process Technol 203:342–348
18. Ciriscioli PR, Springer GS, Wang Q (1991) A technique for determining mechanical properties of thick composite laminates. J Compos Mater 25:1330–1339
19. Korab J, Stefanik P, Kavecky S, Sebo P, Korb G (2002) Thermal conductivity of unidirectional copper matrix carbon fibre composites. Compos Part A: Appl Sci Manuf 33:577–581
20. Bono M, Ni J (2002) A model for predicting the heat flow into the workpiece in dry drilling. J Manuf Sci Eng 124:773–777
21. Weinert K, Kempmann C (2004) Cutting temperatures and their effects on the machining behaviour in drilling reinforced plastic composites. Adv Eng Mater 6:684–689
22. Cui Y, Li H, Li T, Chen L (2018) An accurate thermal performance modeling and simulation method for motorized spindle of machine tool based on thermal contact resistance analysis. Int J Adv Manuf Technol 96:2525–2537
23. Su F, Yuan J, Sun F, Wang Z, Deng Z (2018) Modeling and simulation of milling forces in milling plain woven carbon fiber-reinforced plastics. Int J Adv Manuf Technol 95:4141–4152
24. Kundakcıoğlu E, Lazoglu I, Poyraz Ö, Yasa E, Cizicioğlu N (2018) Thermal and molten pool model in selective laser melting process of Inconel 625. Int J Adv Manuf Technol 95:3977–3984
25. Islam C, Lazoglu I, Altinta Y (2016) A three-dimensional transient thermal model for machining. J Manuf Sci Eng 138:021003-1–021003-17
26. Zhu GP, Bao YJ, Gao H (2012) Research on the drilling temperature field model of the unidirectional carbon fiber epoxy composites. Adv Mater Res 565:478–483
27. Hocheng H, Tsao CC (2003) Comprehensive analysis of delamination in drilling of composite materials with various drill bits. J Mater Process Technol 140:335–339